EasyChair Preprint

№ 8833

Modified Polar Grid-Based Accelerated Image Reconstruction Technique for X-Ray CT

Sudhir Kumar Chaudhary, Pankaj Wahi and Prabhat Munshi

September 15, 2022

Modified Polar Grid-based Accelerated Image Reconstruction Technique for X-ray CT

Sudhir Kumar Chaudhary[1], Pankaj Wahi[2], and Prabhat Munshi[1]

[1]Nuclear Engineering and Technology Programme
Indian Institute of Technology Kanpur
Kanpur, India
email kcsudhir@iitk.ac.in

[2]Department of Mechanical Engineering
Indian Institute of Technology Kanpur
Kanpur, India

ABSTRACT

Image reconstruction by projections is basically a mathematical problem. The speed and accuracy of the reconstruction mainly depend upon, (1) discretization scheme (2) solution technique. Solution by Algebraic Method (AM) is the most promising technique for manufacturing the low-cost (few detectors arrangement) X-ray CT set-up. Slow converging rate and huge memory requirement are the two major drawbacks of AM algorithms. Projection coefficient calculations and their storages are major time and storage-consuming processes of the algebraic methods. Among all algebraic methods, the Multiplicative Algebraic Reconstruction Technique (MART) is more effective because it maximizes the entropy of the image space. The conventional MART algorithm uses square grids (SG) in the discretization process of image reconstruction. In the present work, we employed a modified polar grid to cope with the shortcomings of the MART method. In this new discretization scheme, only the projection coefficients of the first view, need to be calculated. Projection coefficients for other views can be easily calculated by using the symmetries of the modified polar grid. This method significantly reduces the reconstruction time and storage requirement of the MART algorithm. In addition, we also presented the direct method of polar to square grid transformation for the visualization of the reconstructed images. We tested the proposed method to fan-beam geometry for 2D image reconstruction. Structural similarity index (SSIM) and L_2 error are used for quality assessment of the reconstructed images.

Keywords: Cone-beam X-ray, algebraic reconstruction technique, 2-D polar-coordinate image reconstruction

1. INTRODUCTION

Computerized tomography (CT) is an extremely powerful non-invasive technique having tremendous applications in basic/applied sciences and engineering [1]. The common feature in all these applications is the search for a solution to an inverse problem where a given property of a system (e.g. attenuation coefficient for X-ray CT) has to be reconstructed starting from a set of line-integral measurements called projections [2].

There are several different solution methods that are developed to date depending on various tomographic applications. The transform-based algorithms are computationally efficient but produce satisfactory results only for a uniformly distributed large projection data set. The algebraic methods, on the other hand, can be used to produce meaningful results with limited and/or non-uniformly distributed projections [3, 4].

Among several types of algebraic methods, MART algorithms are proven to be efficient and the most accurate method for limited data case applications [5]. It is implemented successfully in different tomographic problems, e.g. temperature measurements with a laser-interferometric setup [6, 7], defects detection in composite plate [8] and analysis of the performance of three-phase pumps used in pumping of oil [9]. These studies have shown that of all these algebraic techniques those based on multiplicative correction are most flexible, and accurate.

The algebraic algorithms in their present form face two major problems: high computational complexity and huge memory requirement to carry out reconstruction [10]. To overcome the shortcoming of AM algorithms, researchers have proposed polar grid (PG) based image reconstructions [11, 12, 13]. These methods significantly reduce the storage and computational cost of the reconstruction. The major drawback of the polar grid-based image reconstruction method is that they rely on certain assumptions which force to use of a large number of projection data for meaningful image formation. Apart from this, the PG scheme has irregular image resolution.

In the present work, we propose a novel Constant Resolution Polar Grid (CRPG) discretization scheme to handle the issues of conventional PG-based methods. Along with this, we also offer a direct CRPG to SG mapping method for proper visualization of the images on the system screen.

2. THEORY

2.1 Constant Resolution Polar Grid

The conventional polar grid is formed by the intersections of various concentric annular rings and radial lines. Each annular ring has the equal number of pixels (see Fig. 1). The space contribution of each pixel increases as we move outward from the center of the image. Thus, the resolution of a conventional polar grid image is highest at the centre and deteriorates along the radial direction. To overcome this shortcoming, we modify the polar grid in such a way that each pixel has the same contribution to the image space. We divide each ring according to the equation $n_p = 4(2n - 1)$, where n_p is the number of pixels in each ring n ($n \in [1, N_r]$, where N_r is the number of rings).

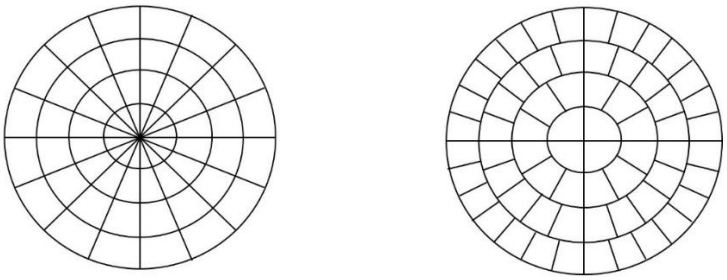

(a) (b)

Fig. 1 Image discretization using polar grids (a) Conventional polar grid (b) Constant resolution polar grid (CRPG).

2.2 Mapping Scheme of Constant Resolution Polar Grid to Square Grid

The visualization screen of the system has a square shaped pixel arrangement. Therefore, we need a mapping method to transform the polar image to square shaped pixel image. Researchers have used interpolation or iterative techniques to perform this operation. In these techniques single grid of polar coordinate system is sampled by many grids of square coordinate. We have shown the numbering strategy of the CRPG discretization scheme in Fig. 2 (a). We separately assign numbers to each grid of a ring starting from zero to n_p (number of grids in ring n). The square grid (SG) coordinate system has been shown in Fig. 2(b) to show the similarity between CRPG and SG. The concentric square rings S_1, S_2, $S_3$and S_4 can be considered as the building block of the square grid. According to the observation, the circular rings of CRPG and their counterpart square rings of SG have the same number of grids. In Fig. 2, circular

rings R_1, R_2, R_3 and R_4 of CRPG and square rings S_1, S_2, S_3 and S_4 of SG have 4, 12, 20 and 28 pixels respectively. Equal number of the grids in the rings of the both geometry, facilitate us to have a perfect one-to-one correspondence. In Fig. 2 (b), we have provided the polar grid number in blue font while the square grid number in black font.

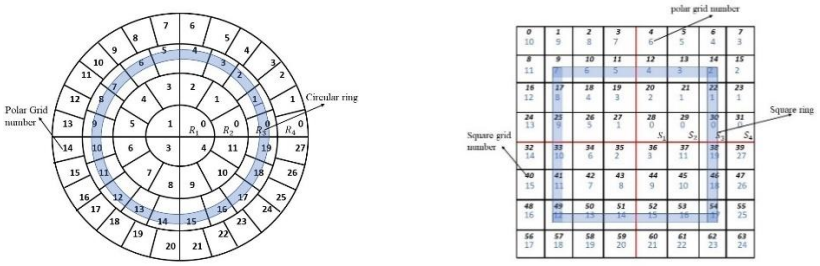

(a) (b)

Fig. 2 Direct mapping Strategy of CRPG to SG (a) Numbering strategy of CRPG (b) Square grid with mapped polar grid numbers in blue font.

2.3 Tracing of Line in the Image Space

The most time-consuming operation of AM algorithms is searching for the path of the line through the image. We have used binary approach to assign the coefficient to the grid. In the binary method, the grids traversed by a line have coefficient one (active grid), other grids have coefficient zero (dead grid). The calculation of coefficients requires to solve the line equation with the circle and radial line of the polar grid. The conventional polar grid algorithms take $O(N^2)$ computation time for tracing the line in the image of size $(N \times N)$. The binary approach facilities to avoid the computation of the line with radial lines thus speeding the coefficient calculation process by $O(N)$.

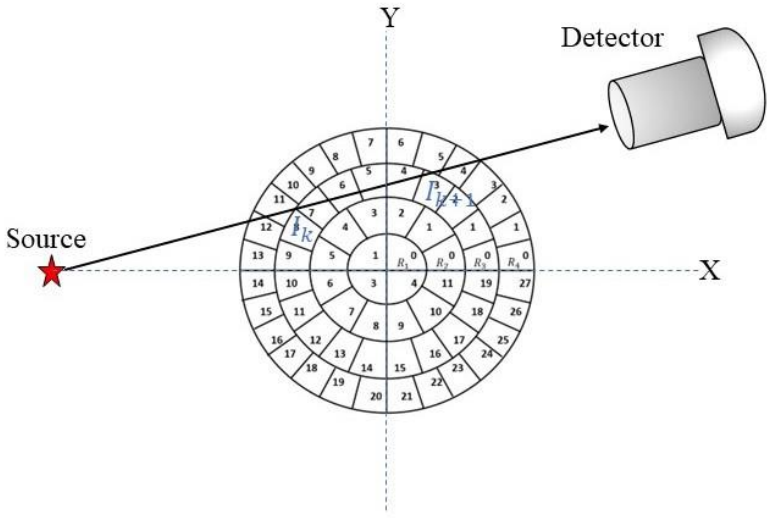

Fig. 3 Schematic of data collection geometry.

We first need to find out the intersection points of the line with the circles of the CRPG and then sort them according to their distance to the source. Two consecutive intersection points I_k and I_{k+1}lies in the same ring in all projections because of symmetry of the CRPG (see Fig. 3). The distance d_k of the point I_k or I_{k+1} decides the ring number R_n of the line segment $I_k I_{k+1}$.

$$d_k = \sqrt{I_{kx}^2 + I_{ky}^2}\,, \tag{1}$$

The ring number R_n of a line segment can be given by,

$$R_n = \frac{d_k}{r_s} \ , \tag{2}$$

where r_s is the ring spacing of the discretization grid (rings are equally spaced).
The angular locations of points I_k and I_{k+1} are required to trace the line segment $I_k I_{k+1}$. The azimuthal angles of these points are given by,

$$\varphi_{I_k} = \tan^{-1}\frac{I_{ky}}{I_{kx}} \quad and \ \ \varphi_{I_{k+1}} = \tan^{-1}\frac{I_{(k+1)y}}{I_{(k+1)x}} \ , \tag{3}$$

Each rings have a different azimuthal step angle $\Delta\varphi_{R_n}$(angle between two consecutive radial planes of ring R_n)

$$\Delta\varphi_{R_n} = \frac{360}{4(2n-1)} \ , \tag{4}$$

Grid number $N_{I_k}$of point I_k , in ring R_n can be find as follows

$$N_{I_k} = \left\lfloor \frac{\varphi_{P_k}}{\Delta\varphi_{R_n}} \right\rfloor . \tag{5}$$

where bracket $\lfloor . . \rfloor$ converts fraction number to the floor number. The grid number of the point I_{k+1} can be find in similar fashion. The grid numbers N_{I_k} and $N_{I_{k+1}}$are sufficient to trace the line segment $I_k I_{k+1}$ in the ring R_n. The line segment $I_k I_{k+1}$passes through all the grids which lies in between these two points.

2.4 Reconstruction Algorithm

Image reconstruction by projections requires to solve the linear equation,

$$P_{p,l} = \sum_v \alpha_{p,l,v} f_v \ , \tag{6}$$

where, $P_{p,l}$ is the measured projection data of line *l* of projection *p*, $\alpha_{p,l,v}$ is the coefficient of line *l* in grid *v* and f_v is the unknown field value of grid *v*. The sparse multiplicative reconstruction technique (Sp-MART) [14] has been used to solve the equation (6). We initialize the solution process by arbitrary field vector $f = (f_0, f_1 \ldots \ldots f_{N^2})$. Equation (6) is used to calculate the numerical projection $\overline{P_{p,l}}$ data using the field vector f. This numerical projection data assist us to update the field vector of the image space using the equation,

$$f_v^{new} = f_v^{old}(1 - \beta \times (1 - \Delta P_{p,l})) \ . \tag{7}$$

where f_v^{new}, f_v^{old} are the new and old field vector and β is the relaxation parameter ($\beta \in [0,2]$). We iterate the loop of equation (6) and (7) until the filed vector stop changing its value.

3. RESULTS

The performance of the proposed method has been evaluated using various types of 2D numerical phantoms namely siemens star, slanted square and Shepp-Logon phantom. The projection data has been calculated using forward projection method for 70 projection views over full $360°$ rotation. The relaxation parameter was set at 0.4 for the back projection process of the image reconstruction. In Fig. 4, we have shown the original and reconstructed images of the numerical phantoms.

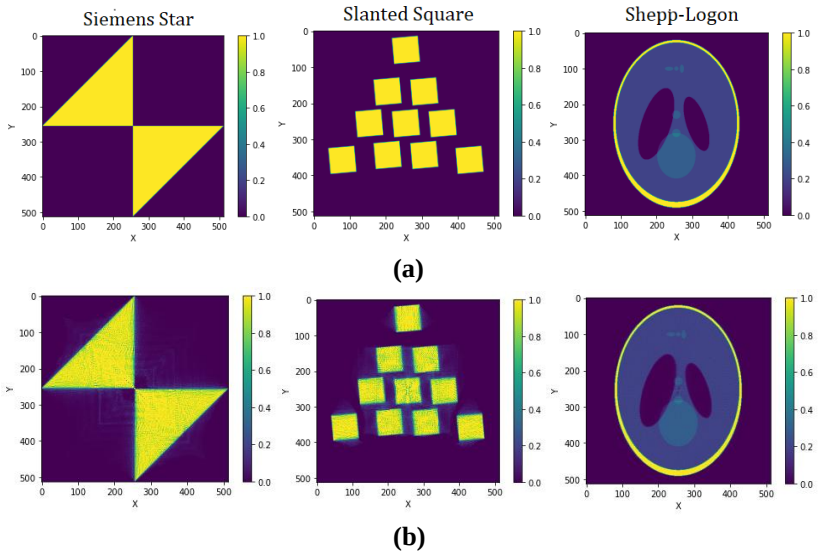

Fig. 4 Reconstruction of numerical phantoms (a) Orginal image (b) Reconstructed image**.**

All the numerical experiments are coded in Python 3.8 and executed with the CPU machine of 64bit, 1.80 GHz, Intel® Core™ i7-8550U. The computational efficiency of the proposed methods have been tested by reconstructing images of different sizes. In Table 1, we have compared the cost of the CRPG based algorithm with the square grid based Sp-MART algorithm [14].

Table 1. Comparison of Total Run Time of the CRPG with Sp-MART algorithm

size	Projections	CRPG based Sp-MART Run Time(seconds)	SG based Sp-MART Run Time (seconds)
128×128	40	45	167
256×256	50	131	390
512×512	70	683	2078

The accuracy of the CRPG reconstruction has been accessed by using various image quality metrics. The mean absolute error (MAE), root mean square error (RMSE) and structural similarity index (SSIM) of the reconstructed images are enumerated in Table 2. It is clear from the Table 2 that the reconstructed images have lower values of MAE, RMSE and higher values of the SSIM. Lower value of the MAE and RMSE indicates better image reconstruction. The high value of SSIM indicates close resemblance of the reconstructed image to the reference image.

Table 2 Quality Assessment Parameters for Image Reconstruction

	Siemens Star	Slanted Squares	Shepp-Logan
MAE	0.07	0.09	0.04
RMSE	0.15	0.19	0.09
SSIM	0.91	0.89	0.93

4. CONCLUSIONS

The current study attempts to address the shortcomings of algebraic methods using the CRPG discretization scheme. The process of line tracing through the image space involves many operations such as multiplications, divisions, integer rounding, and array sorting. In the suggested methods, we just need to trace the lines of the first projection, which requires extremely few operations of multiplications, divisions, and integer rounding. The information of the

first projection view has been utilized to fast tracing the lines of all other projections. Thus the proposed strategy enhances the computational speed by $O(p)$, where p is the number of projections used for the reconstruction. The calculation of forward projection of the line and smearing of the projection values back to the line are performed simultaneously. Therefore, the approaches exercised in the present work also reduce the storage requirement by the factor of p. The shortcoming of radial deterioration of the resolution of the conventional polar grid reconstruction method is also solved by employing CRPG method. In conclusion, we have established a novel mathematical model to speed up the calculations of projection coefficients and reduce the storage requirement of the algebraic algorithms without compromising the image quality.

REFERENCES

[1] P. Munshi, Computerized Tomography for Scientists and Engineers, CRC Press , 2007.

[2] F. Natterer, The Mathematics of Computerized Tomography, Stuttgart: Jhon Wiley & Sons, 1986.

[3] S. K. Chaudhary, K. Rathore, S. Bhattacharjee and P. Munshi, "Tomographic Algorithm for Industrial Plasmas," in *NDE 2017 Conference & Exhibition of the Indian Society for NDT (ISNT)*, Chennai, (2017).

[4] M. Goswami, P. Munshi and A. Khanna, "Non-uniform Arrangement of Emitter-Receiver Pairs Arrangement and Compact Ultrasonic Tomography Setup," *IEEE Sens. J.,* vol. 15, no. 2, pp. 1198-1207, 2014.

[5] Y. Censor, A. R. De-Pierro, T. Elfving, G. T. Herman and A. N. Lusem, "On iterative methods for lineraly constrainted entropy maximization," *Banach Center Publications,* vol. 24, pp. 145-163, 1990.

[6] P. M. V. Subbarao, P. Munshi and K. Muralidhar, "PERFORMANCE EVALUATION OF ITERATIVE TOMOGRAPHIC ALGORITHMS APPLIED TO RECONSTRUCTION OF A THREE-DIMENSIONAL TEMPERATURE FIELD," *Numerical Heat Transfer, Part B: Fundamentals,* vol. 31, pp. 347-372, 1997.

[7] D. Mishra, K. Muralidhar and P. Munshi, "A robust MART algorithm for tomographic applications," *Numer. Heat Transf. B,* vol. 35, no. 4, pp. 485-506, 1999.

[8] N. N. Kishore, P. Munshi, M. A. Ranamale, V. V. Ramakrishna and W. Arnold, "Tomographic Reconstruction of Defects in Composite Plates Using Genetic Algorithms with Cluster Analysis," *J. Res. Nondestruct. Eval.,* vol. 22, no. 1, pp. 31-60, 2011.

[9] S. Shakya, P. Munshi, A. Luke and D. Mewes, "Computerized Tomography Application in Oil Industry using KT-2 Signature," *J. Res. Nondestruct. Eval.,* vol. 26, pp. 61-89, 2015.

[10] M. Bajpai, C. Schorr, M. Maisi, P. Gupta and P. Munshi, "High resolution 3D image reconstruction using the algebraic method for cone-beam geometry over circular and helical trajectories," *NDT E Int.,* vol. 60, pp. 62-69, 2013.

[11] L. Jian, L. Litao, C. Peng, S. Qi and W. Zhifang, "Rotating polar-coordinate ART applied in industrial CT image reconstruction," *NDT & E Int.,* vol. 40, no. 4, pp. 333-336, 2007.

[12] C. Thibaudeau, J. D. Leroux, R. Fontaine and R. Lecomte, "Fully 3D iterative CT reconstruction using polar coordinates," *Med. Phys.,* vol. 40, no. 11, p. 111904, 2013.

[13] S. Zhang, P. Zhou, K. Pan, Z. Liu, Y. Li and T. Sun, "Fast method for computing a system matrix using a polar-coordinate pixel model with concentric annuluses of different radial widths," *Appl. Opt,* vol. 59, no. 36, pp. 11225-11231, 2020.

[14] S. K. Chaudhary and P. Munshi, "Computation and Storage Efficient Sparse MART Algorithm for 2-D, 3-D Reconstruction from Fan Beam, Cone-Beam Projection Data," *Res. Nondestruct. Eval,* vol. 32, no. 3-4, pp. 115-131, 2021.